

Lifecycle-type Matters for Extratropical Cyclone Precipitation Production

Catherine M Naud¹, Jonathan E Martin², Poushali Ghosh², Gregory S Elsaesser¹, James F Booth³ and Derek J Posselt⁴

¹Applied Physics and Applied Mathematics, Columbia University/NASA-GISS, New York, NY.

²Atmospheric and Oceanic Sciences, University of Wisconsin-Madison, Madison, WI.

³Department of Earth and Atmospheric Sciences, City College of New York, NY.

⁴Jet Propulsion Laboratory, California Institute of Technology, Pasadena, CA.

Corresponding author: Catherine M Naud (cn2140@columbia.edu)

Key Points:

- A new method for identifying extratropical cyclone lifecycle-types (occluded vs. non-occluded) is applied to connect them to precipitation.
- Occluded extratropical cyclones produce more precipitation than non-occluded ones because they are collectively more intense
- A unique forcing for ascent allows more efficient precipitation production in occluded than in non-occluded cyclones of similar intensity

19 **Abstract**

20 In the midlatitudes, extratropical cyclones produce the majority of winter precipitation.
21 Precipitation rates and accumulation depend strongly on both the cyclone intensity and the
22 environmental moisture amount. Using five years of the Integrated Multi-satellitE Retrievals for
23 Global Precipitation Measurement (IMERG) product, cyclone-centered composites of surface
24 precipitation rates are compared between cyclones that occlude and those that do not. Occluding
25 cyclones produce greater surface precipitation because they tend to be more intense. When the
26 non-occluding cyclones are selected such that they collectively have similar intensity and
27 moisture amount distributions as the occluding cyclones, precipitation rates at peak intensity are
28 still larger for occluding cyclones. This is because a particular type of forced, frontal-scale,
29 ascent in the occluded thermal ridge, unique to occluded cyclones by virtue of their thermal
30 structure, favors more precipitation. The results demonstrate that life-cycle type (i.e., achieving
31 occlusion versus not) matters for precipitation production in extratropical cyclones.

32 **Plain Language Summary**

33 The weather in the midlatitudes is driven by extratropical cyclones and these storms produce
34 most of the winter precipitation in the northern hemisphere. Both the intensity of the cyclones
35 and the amount of moisture available to them determine how much precipitation they will
36 produce. However, using satellite observations of precipitation averaged in cyclones, it is
37 discovered that the lifecycle-type and associated structural evolution of the cyclones also impacts
38 the precipitation production. Cyclones that undergo occlusion are found to be associated with
39 greater precipitation production than cyclones that do not occlude when the comparison is
40 controlled for similar cyclone intensity and moisture amount. This is because the occluded
41 cyclones are characterized by additional forcing for ascent that boosts precipitation production at

42 the frontal scale. Therefore lifecycle type matters for the amount of precipitation cyclones
43 produce.

44 **1. Introduction**

45 Extratropical cyclones are the main weather features that provide most of the
46 precipitation in the midlatitudes (30-60°N/S), up to 80% in the northern hemisphere winter
47 (Hawcroft et al., 2012; Catto et al., 2012). The precipitation amount produced within an
48 extratropical cyclone depends mostly on the cyclone's intensity and the amount of environmental
49 moisture available to it (Field and Wood, 2007; Pfahl and Sprenger, 2016; Sinclair and Catto,
50 2023). As a result, during its lifecycle, an extratropical cyclone will produce varying amounts of
51 precipitation, with larger amounts earlier in its history when it is actively intensifying than later
52 in its life. In fact, precipitation production maximizes before peak cyclone intensity (Bengtsson
53 et al., 2009; Rudeva and Gulev, 2011; Michaelis et al., 2017). A possible explanation for this
54 behavior is that the latent heat release associated with precipitation production also intensifies
55 the cyclone, though it should be noted that the lag between the two maxima (in precipitation
56 production versus intensity) has been found to be small (Hawcroft et al., 2017; Booth et al.,
57 2018). Booth et al. (2018) found that the time lag is in fact caused by greater amounts of
58 moisture available to the cyclones earlier in their development and intensification phase, as
59 cyclones tend to propagate poleward, towards drier latitudes. However, another potentially
60 important variable that has not been examined in these previous studies is cyclone lifecycle-type;
61 that is, whether the cyclones are occluded or not.

62 Occlusions occur when the cold front encroaches upon and subsequently ascends the warm
63 frontal surface (Stoelinga et al., 2002), producing a 3D wedge of warm and moist air aloft and
64 poleward of the warm front known as the trough of warm air aloft (TROWAL; Crocker et al.,

65 1947; Penner, 1955). The TROWAL manifests as a 3D thermal ridge, connecting the sea-level
66 pressure (SLP) minimum to the peak of the warm sector, i.e., the intersection between surface
67 cold, warm and occluded fronts (Martin, 1998a,b, 1999a,b; Schultz and Vaughan, 2011 and
68 references therein). The length of the associated thermal ridge increases as the occluded cyclone
69 progresses towards eventual decay. Cloud amount and precipitation are maximized in the
70 TROWAL, not along the surface occluded front (Martin, 1998b; Grim et al, 2007; Han et al.
71 2007; Naud et al., 2024). Therefore, occluded cyclones can produce large amounts of
72 precipitation, and when over land cause crippling snow accumulations (Schultz and Mass, 1993;
73 Martin 1998a, 1998b, 1999a, 1999b). Martin (1999b) showed that the characteristic lengthening
74 of the occluded thermal ridge is forced by non-frontogenetical geostrophic deformation that
75 differentially rotates the baroclinic zones that straddle the thermal ridge. In a substantial portion
76 of the occluded sector, the quasi-geostrophic (QG) vertical motion ω is attributable to this
77 specific process, which operates exclusively in occluded cyclones.

78 Despite the importance of the presence of a thermal ridge for the overall cloud and
79 precipitation produced in occluded cyclones (Naud et al., 2024), it is not presently known
80 whether the lifecycle-type (occluding versus non occluding cyclones) matters for precipitation
81 production in extratropical cyclones *on average*. To explore this question, the Integrated Multi-
82 satellitE Retrievals for Global Precipitation Measurement (IMERG; Huffman et al. 2020; 2023)
83 surface precipitation product and a database of cyclone tracks are combined to explore
84 differences in precipitation production in cyclones that occlude as compared with those that do
85 not.

86

87 **2. Datasets and methodology**

88 To conduct the analysis, we use a database of extratropical cyclones and focus on a 5-year
89 period (2014-2018). We consider here only northern hemisphere cyclones during the winter
90 months (December, January, February). The database is described below, along with the
91 precipitation data, the methodology used to pair cyclones and precipitation, and finally the
92 reanalysis data used to help characterize the cyclones.

93 2.1 Extratropical cyclones selection and subsetting

94 We use a publicly available database of extratropical cyclones (Naud et al., 2023) that
95 provides the location of cyclone centers and their corresponding minima in sea level pressure
96 (SLP) every 6 hours from first to last detection (hereafter referred to as a track). The algorithm of
97 Bauer and Del Genio (2006) was used for the tracking, with ERA-interim sea level pressure
98 fields as input. Each cyclone track is assessed to establish whether the cyclone was occluded at
99 some point in time. Occlusion assessment was performed using the algorithm described in Naud
100 et al. (2023), where the identification relies on the presence of an occluded thermal ridge. This
101 feature's quantitative diagnostic is computed by calculating the divergence of the unit vector of
102 the 1000-500 hPa thickness gradient near the cyclone center as the system progresses in time
103 through its lifecycle (with convergence indicating an occluded state). We separate the cyclone
104 tracks that are identified as being occluded at some point in time ("Occluded Cyclones") from
105 those that never are ("Non-occluded Cyclones").

106 For each track in each category, we also mark the time at which the cyclone reaches its peak
107 intensity, defined here as the time when the cyclone reaches its minimum in central SLP. This is
108 used to ensure the cyclones are at a similar stage in their lifecycle when comparing occluded to

109 non-occluded cyclones. While peak intensity can be defined with other metrics (e.g. wind or
110 vorticity), here we only need to ensure that the definition is consistent for both populations.
111 Although some cyclones might be identified as occluded only after the time of peak intensity,
112 they are still included in the “occluded cyclones” group. For the 2014-2018 time period, a total
113 of 1341 cyclones at peak intensity were identified, 162 of which occluded (i.e., about 12% of the
114 entire cyclone population). By design, the occlusion identification method is conservative,
115 implying that some cyclones categorized as non-occluded might in fact occlude at some point;
116 however, the occlusion might be short-lived or the detection signal weak.

117 2.2 Precipitation data

118 For surface precipitation rates, we use the Integrated Multi-satellitE Retrievals for Global
119 Precipitation Measurement (GPM) mission (IMERG; Huffman et al., 2020; 2023) version 7
120 product. This product reports surface precipitation rates every 30 minutes on a $0.1^\circ \times 0.1^\circ$ grid
121 using passive microwave rainfall and infrared data from a constellation of satellites. These
122 different datasets are intercalibrated using the GPM core observatory radiometer data. The “Final
123 Run” product is further calibrated using monthly-mean gauge data. For each cyclone considered
124 in our analysis, we collect the IMERG data in a 6-hour-long time window centered on the time of
125 cyclone identification (i.e., we aggregate the prior and post six 30-minutes IMERG time steps).
126 We retain only IMERG grid cells that are within 1500 km of each cyclone center, and then
127 project the grid cells onto a rectangular grid centered on the cyclone SLP point (with cell
128 projection locations based on the distance an IMERG cell is from the cyclone center). The
129 rectangular grid has a domain of ± 1500 km in the meridional and zonal directions, and 200 km
130 spatial resolution. The IMERG data is averaged in each 200 km cell, from its native resolution.
131 This regridding procedure is fully described in Naud et al. (2018).

132 2.3 Cyclone properties

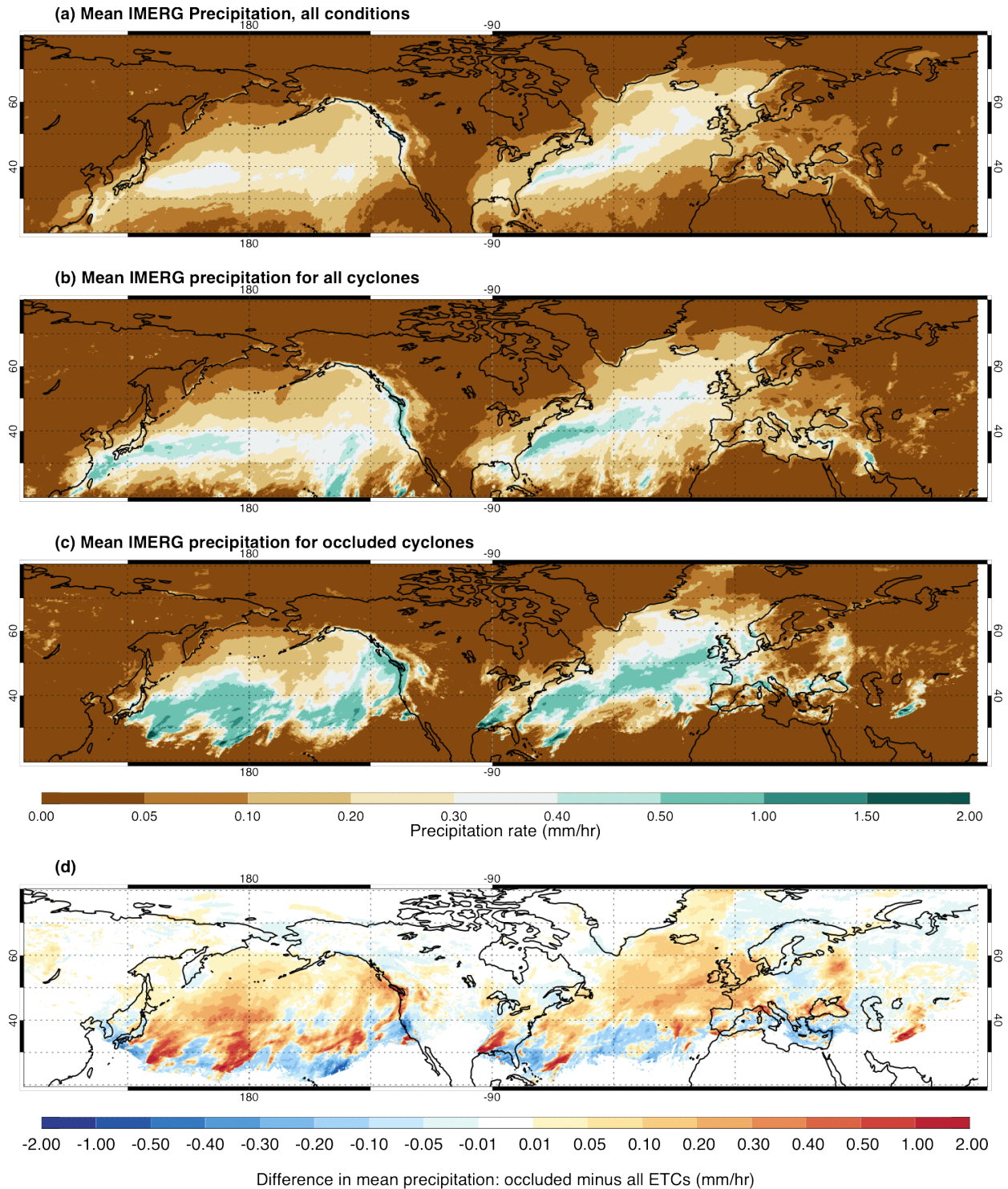
133 For each cyclone at peak intensity in the two categories (occluded vs. non-occluded), we
134 collect coincident Modern Era Retrospective Analysis for Research and Applications version 2
135 (MERRA-2; Gelaro et al., 2017) 500 hPa vertical velocity ω (where ascending) and precipitable
136 water (PW). We project these two fields onto a cyclone-centered grid following the approach for
137 IMERG precipitation data projection (see above). Additionally, we calculate the mean PW and
138 mean upward vertical velocity within a 1500 km radius centered on the SLP minimum. These
139 two numbers characterize the environmental moisture and the ascent strength of the cyclones
140 which are both important for precipitation production. To better characterize cyclone intensity,
141 we include calculations of the mean MERRA-2 surface wind speed in the same circular region.
142 To analyze the thermal structure of the cyclones, we also collect the 700 hPa equivalent potential
143 temperature using MERRA-2 temperature and specific humidity fields, and use the same
144 regridding routine to map these fields to the cyclones.

145 **3. Mean precipitation rates in the northern hemisphere winter**

146 Before we examine precipitation within the cyclones, we first examine where and to what
147 extent cyclones contribute to northern hemisphere winter precipitation. For this we first average
148 IMERG DJF precipitation rates at their native resolution for 2014-2018 in all conditions (Fig 1a).
149 The 5-year mean precipitation is clearly greatest in the storm track regions of the north Atlantic
150 and Pacific as expected (c.f. Hawcroft et al., 2012). Next, we collect IMERG precipitation rates
151 accumulated over 6 hours centered on the times of cyclone identification (00, 06, 12, 18 UT),
152 and compute a conditional average, where we only consider the rainfall reported within the
153 identified cyclone of radius 1500 km before we calculate the 5-year mean (i.e., we neglect all
154 other times/locations). The 5-year mean of IMERG precipitation rate for regions with a cyclone

155 (Fig 1b) resembles the map of all conditions, but the maximum in mean precipitation rate within
156 the storm tracks is now much larger. Finally, we average the precipitation in a similar fashion,
157 but now, only consider IMERG pixels associated with cyclones flagged as being occluded (Fig.
158 1c). For these systems, the precipitation is more intense everywhere in the storm tracks, with
159 notably large rates in coastal regions of northern Europe, the eastern United States and Canada,
160 the Pacific Northwest, and northeast Asia. A map of the differences in mean precipitation rate
161 between occluded cyclones and all cyclones (Fig. 1d) suggests that most of the storm track has
162 more intense precipitation in the presence of an occluded cyclone. One exception is the southern
163 edge of the study area where precipitation is less intense when occluded cyclones are present.
164 This could be a result of the fact that occluded cyclones often “cut off” at upper tropospheric
165 levels thereby limiting the equatorward export of cold air and the associated frontogenetically
166 forced precipitation that accompanies such excursions.

167



168

169 **Figure 1:** Mean IMERG precipitation for 2014-2018 in the northern hemisphere winter for (a)
 170 all time steps, (b) 6-hourly periods when a cyclone is identified at the middle time step with an
 171 area of influence defined as a 1500 km radius centered on each cyclone's center, (c) 6-hourly

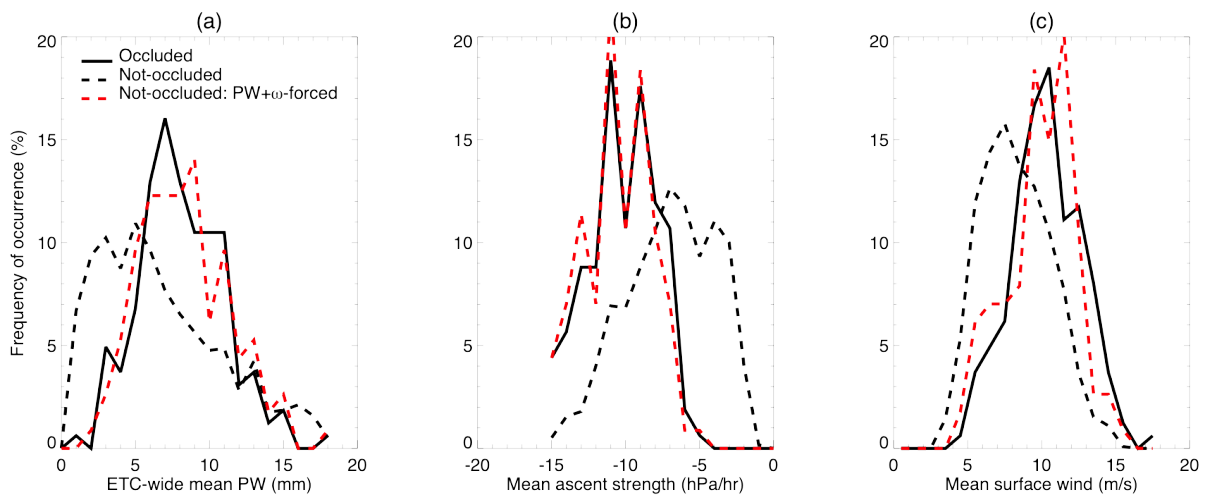
172 periods when an occluded cyclone is present and (d) difference in mean precipitation between (c)
173 and (b).
174

175 **4. Cyclone-centered precipitation composites: occluded versus non-occluded cyclones at** 176 **peak intensity**

177 As mentioned earlier, precipitation in extratropical cyclones typically depends on the amount
178 of environmental moisture available to them, usually measured with PW, and on their intensity
179 (e.g. Field and Wood, 2007; Pfahl and Sprenger, 2016). Typically, cyclone intensity is gauged
180 with wind speed, SLP minimum, or 850 hPa vorticity, but here we choose the 500 hPa vertical
181 velocity (ω) averaged across the region of ascent. This metric more directly characterizes the
182 necessary lift for precipitation production. To better understand the differences in Figure 1, we
183 first examine the differences across occluded and non-occluded cyclones in terms of moisture
184 and intensity. To do so, we examine the distribution of mean cyclone-wide PW, mean ascent
185 strength and mean surface wind in the occluded and non-occluded cyclone subgroups for our
186 subset of cyclones at peak intensity (Fig. 2). Cyclones that occlude tend to be more intense (Fig.
187 2c), and have stronger ascent strength overall (Fig. 2b). They also display a fairly narrow
188 distribution of PW compared to non-occluded cyclones (Fig. 2a), presumably because they tend
189 to occur in a narrower latitude band than the more numerous non-occluding cyclones (Naud et
190 al., 2023). All three distributions suggest that precipitation would be more intense in occluded
191 than non-occluded cyclones, consistent with Figure 1.

192 But to get a better sense of the importance of occlusion alone for precipitation production, we
193 subset the more numerous non-occluded cyclones such that they have as similar as possible
194 distributions of both ascent strength and PW as their occluded counterparts. To do this, we
195 arrange the non-occluded cyclones in 1 hPa/hr-wide ascent strength bins and, using a random

196 number generator, randomly remove (non-occluded) cyclones in each ascent strength bin until
 197 we obtain the same number as for occluded cyclones in the same ascent strength bin. We then
 198 use this new set of non-occluded cyclones to similarly force the PW distribution (arranged in 1
 199 mm bins) to match that of occluded cyclones. This is done by counting remaining non-occluded
 200 cyclones in each PW bin and when that number exceeds that of occluded cyclones, again apply a
 201 random number generator to remove the excess. This gives a subset of 114 non-occluded
 202 cyclones that collectively have very similar mean PW, ascent strength and surface wind
 203 distributions as the occluded cyclones (dashed red line in Fig 2). This is the subset we use next
 204 for the lifecycle-type mean precipitation rates comparison.



205

206 **Figure 2:** Distribution of mean (a) PW, (b) 500 hPa ascent strength and c) surface wind speed
 207 for occluded cyclones (solid black line), non-occluded cyclones (dashed black line) and the
 208 subset of non-occluded cyclones that have a similar PW and ascent strength distributions (dashed
 209 red line) to occluded cyclones.

210

211 When comparing cyclone-centered composites of precipitation, for similar PW and ascent
 212 strength distributions, precipitation is larger for occluded than non-occluded cyclones (Figure 3a
 213 vs. 3b). For both types of cyclones, the maximum in precipitation appears related to the structure

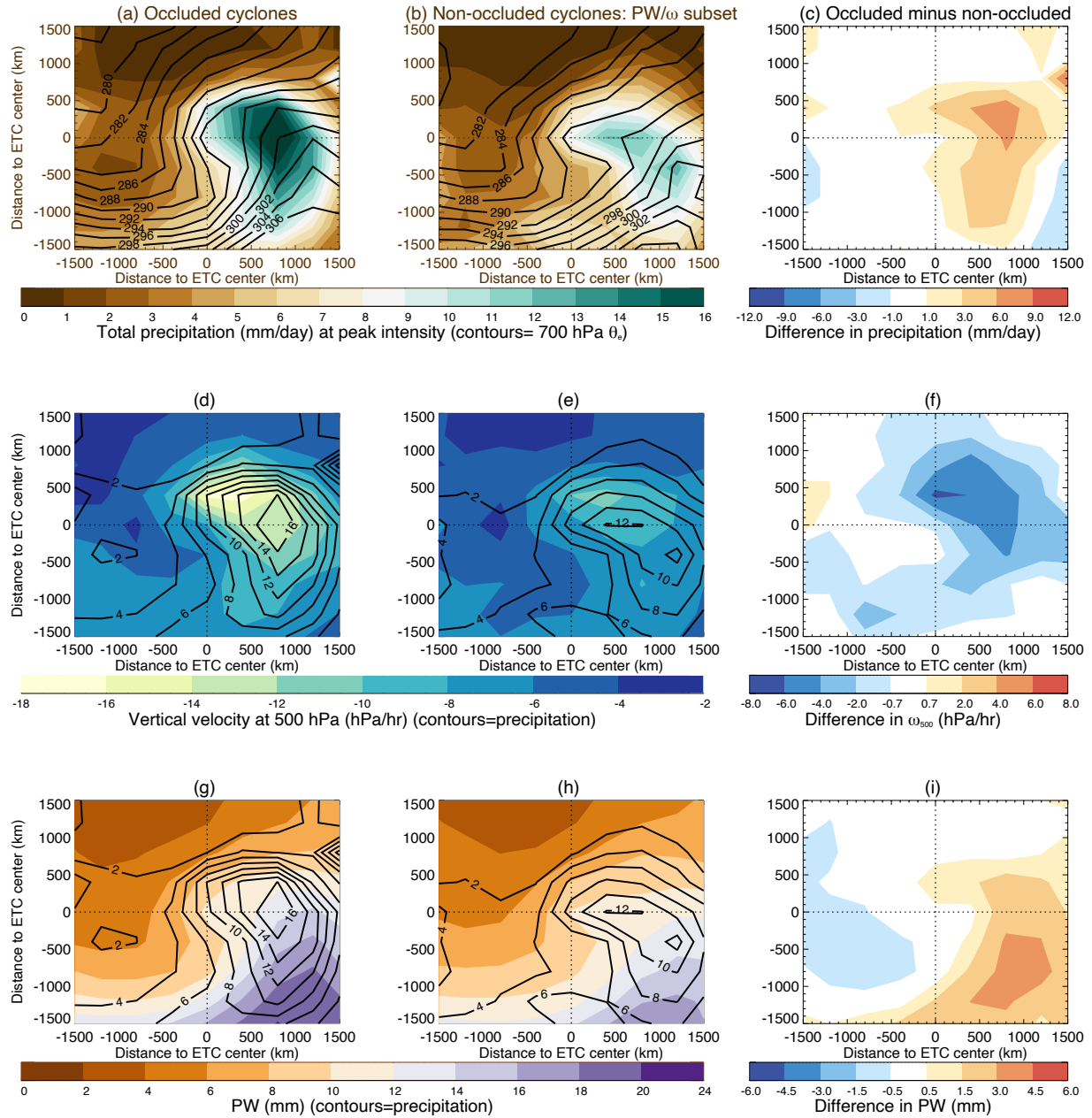
214 of the 700 hPa equivalent potential temperature θ_e spatial distribution (Figs. 3a, 3b), with
215 maxima occurring along the thermal ridge for the occluded cyclones (Fig. 3a), and along the
216 warm front for the unoccluded ones (Fig. 3b). The difference in precipitation (Fig 3c) is
217 therefore maximum along the occluded thermal ridge, i.e., the axis of maximum θ_e , evident in
218 Fig. 3a.

219 When examining the actual composites of 500 hPa vertical velocity (Fig. 3d, 3e), while the
220 cyclone-wide mean ascent is forced to be the same in the two populations, the maximum in
221 ascent strength is larger for occluded cyclones (up to between 6 and 8 hPa/hr difference, Fig. 3f).
222 The region of ascent is also more compact for occluded cyclones, as revealed by sharper decline
223 in ascent strength from east to west than for non-occluded cyclones (Fig. 3f). The significantly
224 stronger ascent also aligned along the occluded thermal ridge is consistent with Martin (1999b)'s
225 analysis of three individual occluded cyclones that revealed strong frontal scale ascent in the
226 thermal ridge region associated with the non-frontogenetical geostrophic deformation component
227 of the Q-vector.

228 The cyclone-centered composites of PW reveal that while on average PW is similar in the
229 two cyclone populations, in fact the western half of the non-occluded cyclones is wetter, but the
230 warm sector is slightly drier than that for occluded cyclones. This disparity in the distribution of
231 moisture matches the difference in ascent spatial distribution and confirms that the warm sector
232 is less expansive for the occluded cyclones. The frontal scale forcing for ascent as demonstrated
233 in Martin (1999b), mobilized *only* in the presence of the thermal ridge, is likely responsible for
234 the additional precipitation that distinguishes occluded from non-occluded cyclones with
235 equivalent precipitable water and synoptic scale ascent.

236 The composites imply that occluded cyclones are more efficient at producing precipitation
237 for a given amount of moisture and cyclone intensity than non-occluded cyclones, making the
238 lifecycle-type an important factor for precipitation production in cyclones. To quantify the
239 additional precipitation, we use the composites to calculate the mean precipitation rates in a
240 series of circular regions around the cyclone centers at radii of 500 km, 1000 km and 2000 km.
241 For occluded cyclones, the mean precipitation in each circle is: 8.9, 7.5, and 4.9 mm/hr,
242 respectively. For non-occluded cyclones, we obtain: 7.1, 5.3, and 4.1 mm/hr. Regardless of the
243 region's size, the mean precipitation rate is always greater for occluded cyclones. The greatest
244 difference relative to non-occluded cyclones is achieved for the 1000 km radius region, that
245 includes the peak of the warm sector area, with a 42% excess in precipitation for occluded versus
246 non-occluded cyclones.

247



248

249 **Figure 3:** Cyclone-centered composites of (a, b) IMERG precipitation, (d, e) MERRA-2 500 hPa
 250 vertical velocity where ascending and (g, h) MERRA-2 PW in (a, d, g) occluded and (b, e, h)
 251 non-occluded cyclones of similar mean PW and ascent strength when at peak intensity in the
 252 northern hemisphere winter months of 2014-2018. Differences between occluded and non-
 253 occluded cyclones in (c) precipitation, (f) 500 hPa vertical velocity where ascending and (i) PW.
 254 Overplotted as black contours in (a, b) are the corresponding composites of 700 hPa Equivalent
 255 potential temperatures θ_e in 3 K increments from 278 K; and in (d, e, g, h) the corresponding
 256 IMERG precipitation rates in mm/day in 2 mm/day increments from 2 to 14 mm/day.

257 **5. Conclusions**

258 Using IMERG precipitation rates and a database of extratropical cyclones, precipitation
259 production in extratropical cyclones is explored as a function of lifecycle-type. A 5-year mean of
260 IMERG precipitation rates in Northern Hemisphere winter shows that most of the precipitation is
261 produced in extratropical cyclones, but the mean is larger if the cyclones undergo occlusion
262 during their lifecycles. When examining cyclone-centered mean precipitation rates for cyclones
263 that have reached their peak intensity, occluding cyclones have larger rates than non-occluding
264 ones. The differences are driven by the greater average intensity of occluded cyclones. But when
265 we force the set of non-occluded cyclones to collectively exhibit a similar distribution of ascent
266 strength and PW as the set of occluded cyclones, the difference in mean cyclone-centered
267 precipitation rates remains: occluded cyclones precipitate up to 42% more than non-occluded
268 ones.

269 Cyclones that occlude develop a characteristic thermal ridge that connects the SLP
270 minimum to the peak of the warm sector (defined as the intersection between cold, warm and
271 occluded fronts). The development of a such a feature mobilizes a frontal scale ascent from non-
272 frontogenetical deformation (Martin, 1999b) that underlies the cloud and precipitation
273 production along the axis of the thermal ridge. This thermal structure and its attendant ascent
274 region are entirely absent in non-occluded cyclones. Martin (1999b) demonstrated this
275 mechanism for three separate occluded cyclones, and found that its operation had a strong
276 correspondence with intense precipitation. In the present analysis, the observed mean
277 precipitation in 162 occluded cyclones over a full 5-winter period is similarly maximized in the
278 thermal ridge region. Furthermore, our results indicate that, when controlling for mean ascent

279 strength and moisture availability over a broad, cyclone-centered domain, occluded cyclones are
280 more efficient at producing precipitation.

281 Overall, these results point out that lifecycle-type needs to be taken into account when
282 considering how a warmer climate may change the extratropical cyclone's contribution to
283 midlatitude precipitation. Earth System Models *can* simulate the structure and evolution of
284 occluded cyclones accurately (Naud et al., 2025). They could help investigate to what extent
285 future precipitation changes arise from perturbations in the character of precipitation (i.e.,
286 convective, including elevated, versus stratiform precipitation) in different lifecycle types.
287 Precipitation associated with extratropical cyclones is expected to increase in a warmer climate,
288 mostly due to an increase in environmental moisture (Yettella and Kay, 2017). The associated
289 increase in latent heat release was found to have minimal impact on the cyclones intensity
290 (Sinclair and Catto, 2023), but it is not known if it can instead affect the development of
291 occlusions (Posselt and Martin, 2004). Therefore, the present study suggests that faithful
292 projections of mid-latitude wintertime precipitation changes in a warmer climate will depend
293 upon accurate assessment of how the frequency of occluded cyclones changes as warming
294 progresses.

295 **Acknowledgments**

296 The work was funded by the NASA CloudSat-CALIPSO science team recompetete program, grant
297 number 80NSSC20K0085. CMN and DJP received additional funding from the NASA
298 Modeling, Analysis and Prediction (MAP) program, grant number 80NSSC21K1728 and GSE
299 from the NASA MAP Program and APAM-GISS Cooperative Agreement 80NSSC18M0133,
300 NASA Precipitation Measurement Missions grant 80NSSC22K0609, and the NASA PolSIR
301 project (80LARC24CA001). A portion of this research was conducted at the Jet Propulsion

302 Laboratory, California Institute of Technology, under a contract with the National Aeronautics
303 and Space Administration (NASA) 80NM0018D0004..

304

305 **Open Research**

306 The cyclone database is publicly available through [https://data.giss.nasa.gov/storms/obs-](https://data.giss.nasa.gov/storms/obs-etc/)
307 [etc/](https://data.giss.nasa.gov/storms/obs-etc/). IMERG and MERRA-2 data can be obtained through the NASA Goddard Earth Science
308 Data and Information Services Center <https://disc.gsfc.nasa.gov/datasets>
309 Global Modeling and Assimilation Office (GMAO) (2015), MERRA-2 tavg1_2d_slv_Nx: 2d,1-
310 Hourly,Time-Averaged,Single-Level,Assimilation,Single-Level Diagnostics V5.12.4, Greenbelt,
311 MD, USA, Goddard Earth Sciences Data and Information Services Center (GES DISC),
312 Accessed: 01-2024, [10.5067/VJAFPLI1CSIV](https://doi.org/10.5067/VJAFPLI1CSIV)

313 Global Modeling and Assimilation Office (GMAO) (2015), MERRA-2 tavg3_3d_asm_Nv:
314 3d,3-Hourly,Time-Averaged,Model-Level,Assimilation,Assimilated Meteorological Fields
315 V5.12.4, Greenbelt, MD, USA, Goddard Earth Sciences Data and Information Services Center
316 (GES DISC), Accessed: 01-2024, [10.5067/SUOQESM06LPK](https://doi.org/10.5067/SUOQESM06LPK)

317 Huffman, G.J., E.F. Stocker, D.T. Bolvin, E.J. Nelkin, Jackson Tan (2023), GPM IMERG Final
318 Precipitation L3 Half Hourly 0.1 degree x 0.1 degree V07, Greenbelt, MD, Goddard Earth
319 Sciences Data and Information Services Center (GES DISC), Accessed: 01-2024,
320 [10.5067/GPM/IMERG/3B-HH/07](https://doi.org/10.5067/GPM/IMERG/3B-HH/07)

321

322 **References**

323 Bauer, M. and A. D. Del Genio, 2006: Composite analysis of winter cyclones in a GCM:
324 Influence on climatological humidity. *J. Climate*, 19, 1652-1672.

325 Bengtsson L., K. I. Hodges, and N. Keenlyside, 2009: Will extratropical storms intensify in a
326 warmer climate? *J. Climate*, 22, 2276-2301, doi:10.1175/2008JCLI2678.1.

327 Booth J. F., C. M. Naud and J. Jeyaratnam, 2018: Extratropical cyclone precipitation life cycles:
328 a satellite-based analysis. *Geophys. Res. Lett.* **45**, no. 16, 8647-8654,
329 doi:10.1029/2018GL078977

330 Catto, J. L., C. Jakob, G. Berry and N. Nicholls 2012: Relating global precipitation to
331 atmospheric fronts. *Geophys. Res. Lett.*, 39, L10805, doi: 10.1029/2012GL051736.

332 Crocker, A., W. L. Godson, and C. M. Penner, 1947: Frontal contour charts. *J. Atmos. Sci.*, 4 (**3**),
333 95–99.

334 Field P. R. and R. Wood, 2007: Precipitation and cloud structure in midlatitude cyclones. *J.*
335 *Climate*, 20, 233-254, doi:10.1175/JCLI3998.1.

336 Gelaro, R., McCarty, W., Suarez, M. J., Todling, R., Molod, A., Takacs, L., ... Zhao,
337 B. (2017). The Modern-Era Retrospective Analysis for Research and Applications, Version 2
338 (MERRA-2). *J. Climate*, **30(14)**, 5419–5454.

339 Grim J. A., R. M. Rauber, M. K. Ramamurthy, B. F. Jewett and M. Han, 2007: High-resolution
340 observations of the Trowal-Warm-frontal region of two continental winter cyclones. *Month.*
341 *Weath. Rev.*, 135, 1629-1646, doi:10.1175/MWR3378.1.

342 Han M., R. M. Rauber, M. K. Ramamurthy, B. F. Jewett and J. A. Grim, 2007: Mesoscale
343 dynamics of the TROWAL and warm-frontal regions of two continental winter cyclones.
344 *Month. Weath. Rev.* 135, 1647-1670, doi: 10.1175/MWR3377.1.

345 Hawcroft M. K., L. C. Shaffrey, K. I. Hodges and H. F. Dacre, 2012: How much northern
346 hemisphere precipitation is associated with extratropical cyclones? *Geophys. Res. Lett.*, 39,
347 L24809, doi:10.1029/2012GL053866.

348 Hawcroft, M., Dacre, H., Forbes, R., K. Hodges, L. Shaffrey, and T. Stein, 2017: Using satellite
349 and reanalysis data to evaluate the representation of latent heating in extratropical cyclones in
350 a climate model. *Clim. Dyn.*, 48, 2255–2278

351 Huffman, G. J. (2020). Algorithm Theoretical Basis Document (ATBD) version 5.2 NASA
352 Global Precipitation Measurement (GPM) Integrated multi-satellitE retrieval for GPM
353 (IMERG). Retrieved from [https://gpm.nasa.gov/sites/default/files/2020-](https://gpm.nasa.gov/sites/default/files/2020-05/IMERG_ATBD_V06.3.pdf)
354 [05/IMERG_ATBD_V06.3.pdf](https://gpm.nasa.gov/sites/default/files/2020-05/IMERG_ATBD_V06.3.pdf)

355 Huffman, G.J., E.F. Stocker, D.T. Bolvin, E.J. Nelkin, Jackson Tan (2023), GPM IMERG Final
356 Precipitation L3 Half Hourly 0.1 degree x 0.1 degree V07, Greenbelt, MD, Goddard Earth
357 Sciences Data and Information Services Center (GES DISC), Accessed: 01-2024,
358 [10.5067/GPM/IMERG/3B-HH/07](https://disc.gsfc.nasa.gov/datasets/GPM/IMERG/3B-HH/07).

359 Martin, J. E., 1998a: The structure and evolution of a continental winter cyclone. Part I: Frontal
360 structure and the occlusion process. *Mon. Wea. Rev.*, 126 (2), 303–328.

361 Martin, J.E., 1998b: The structure and evolution of a continental winter cyclone. Part II: Frontal
362 forcing of an extreme snow event. *Mon. Wea. Rev.*, 126 (2), 329–348.

363 Martin, J.E., 1999a: Quasi-geostrophic forcing of ascent in the occluded sector of cyclones and
364 the trowal airstream. *Mon. Wea. Rev.*, 127, 70–88.

365 Martin, J.E., 1999b: The separate roles of geostrophic vorticity and deformation in the mid-
366 latitude occlusion process. *Mon. Wea. Rev.*, 127, 2404–2418.

367 Michaelis A. C., J. Willison, G. M. Lackmann and W. A. Robinson, 2017: Changes in winter
368 north Atlantic extratropical cyclones in high-resolution regional pseudo-global warming
369 simulations. *J. Climate*, 30, 6905-6925, doi:10.1175/JCLI-D-16-0697.1

370 Naud, C.M., J.F. Booth, M. Lebsock, and M. Greco, 2018: Observational constraint for
371 precipitation in extratropical cyclones: Sensitivity to data sources. *J. Appl. Meteorol.*
372 *Climatol.*, **57**, no. 4, 991-1009, doi:10.1175/JAMC-D-17-0289.1.

373 Naud C. M., G. S. Elsaesser, J. E. Martin, P. Ghosh, D. J. Posselt and J. F. Booth, 2025: How
374 well does an Earth Sytem Model represent the occlusion of extratropical cyclones? *J.*
375 *Climate*, in press, JCLI-D-24-0252.

376 Naud, C.M., P. Ghosh, J.E. Martin, G.S. Elsaesser, and D.J. Posselt, 2024: A CloudSat-
377 CALIPSO view of cloud and precipitation in the occluded quadrants of extratropical
378 cyclones. *Q. J. Roy. Meteorol. Soc.*, early on-line, doi:10.1002/qj.4648.

379 Naud, C.M., J.E. Martin, P. Ghosh, G.S. Elsaesser, and D.J. Posselt, 2023: Automated
380 identification of occluded sectors in midlatitude cyclones: Method and some climatological
381 applications. *Q. J. Roy. Meteorol. Soc.*, 149 1990-2010, doi:10.1002/qj.4491.

382 Penner, C., 1955: A three-front model for synoptic analyses. *Quart. J. Roy. Meteor. Soc.*, 81
383 (347), 89–91.

384 Pfahl, S. and M. Sprenger, 2016: On the relationship between extratropical cyclone precipitation
385 and intensity. *Geophys. Res. Lett.*, 43 (4), 1752–1758, doi:10.1002/2016GL068018.

386 Posselt, D. J., and J. E. Martin, 2004: The Effect of Latent Heat Release on the Evolution of a
387 Warm Occluded Thermal Structure., *Mon. Wea. Rev.*, **132**, 578-599.

388 Rudeva I. and S. K. Gulev, 2011: Composite analysis of North Atlantic extratropical cyclones in
389 NCEP-NCAR reanalysis data. *Month. Weath. Rev.*, **139**, 1419-1446,
390 doi:10.1175/2010MWR3294.1

391 Schultz D. M., and C. F. Mass, 1993: The occlusion process in a midlatitude cyclone over land.
392 *Month. Weath. Rev.*, 121, 918-940.

393 Schultz, D.M., and G. Vaughan, 2011: Occluded fronts and the occlusion process: A fresh look
394 at conventional wisdom. *Bull. Amer. Meteor. Soc.*, 92 (4), 443–466.

395 Sinclair, V. A. and Catto, J. L., 2023: The relationship between extra-tropical cyclone intensity
396 and precipitation in idealised current and future climates, *Weather Clim. Dynam.*, 4, 567–
397 589, <https://doi.org/10.5194/wcd-4-567-2023>.

398 Stoelinga M. T., J D. Locatelli and P. V. Hobbs, 2002: Warm occlusions, cold occlusions and
399 forward tilting cold fronts. *Bull. Amer. Meteorol. Soc.*, 83, 709-721.

400 Yettella V. and J. E. Kay, 2017: How will precipitation change in extratropical cyclones as the
401 planet warms? Insight from a large initial condition climate model ensemble. *Clim. Dyn.* 49,
402 1765-1781. Doi:10.1007/s00382-016-3410.2.

403

404